Spinning black hole in a fluid

Surojit Dalui,[1,*] Arpan Krishna Mitra,[2,†] Deeshani Mitra,[3,‡] and Subir Ghosh[3,§]

[1]*Department of Physics, Shanghai University, 99 Shangda Road, Baoshan District, Shanghai 200444, People Republic of China*

[2]*Aryabhatta Research Institute of Observational Sciences (ARIES), Manora Peak Nainital—263001, Uttarakhand, India*

[3]*Indian Statistical Institute, 203, Barrackpore Trunk Road, Kolkata 700108, India*

(Received 15 August 2023; accepted 21 February 2024; published 18 March 2024)

In this paper, we propose a new analog gravity example—a spinning (or Kerr) black hole in an extended fluid model; the latter was derived in an earlier work [A. K. Mitra and S. Ghosh, Divergence anomaly and Schwinger terms: Towards a consistent theory of anomalous classical fluids, Phys. Rev. D **106**, L041702 (2022).] by two of the present authors. The fluid model receives Berry curvature contributions and applies to electron dynamics in condensed matter lattice systems in the hydrodynamic limit. We construct the acoustic metric for sonic fluctuations that obey a structurally relativistic wave equation in an effective curved background. In a novel approach of dimensional analysis, we have derived explicit expressions for effective mass and angular momentum per unit mass in the acoustic metric (in terms of fluid parameters), to identify with corresponding parameters of the Kerr metric. The spin is a manifestation of the Berry curvature-induced effective noncommutative structure in the fluid. Finally we put the Kerr black hole analogy in a robust setting by revealing explicitly the presence of horizon and ergoregion for a specific background fluid velocity profile. We also show that near horizon behavior of the phase-space trajectory of a probe particle agrees with Kerr black hole analogy. In a fluid dynamics perspective, the presence of a horizon signifies the wave blocking phenomenon.

DOI: 10.1103/PhysRevD.109.064055

I. INTRODUCTION

Analog gravity [1] started with the work of Unruh [2], who showed that first-order fluctuations in irrotational, nonviscous, barotropic flow obey a structurally relativistic massless scalar wave equation in an effectively curved background, with an acoustic metric (AM), comprising of fluid flow parameters (for diverse models, see [3,4]). AM reveals black/white holelike features in velocity space, known as wave blocking in fluid dynamics [5].

In this paper, we construct a new AM, (in the framework of [2]), in an extended fluid model with the Berry curvature effects, derived in [6]. This phase space describes semiclassical electron dynamics in a magnetic Bloch band, with periodic potential in an external magnetic field and Berry curvature [7]. This fluid dynamics is relevant in electron hydrodynamics in condensed matter, where electron flow obeys hydrodynamic laws instead of Ohmic [8]. Generically electrons in metals act as nearly-free Fermi gas with a large mean free path for electron-electron collision. Recently hydrodynamic regime was achieved in extremely pure, high quality, electronic materials—especially graphene [9], layered materials with very high electrical conductivity such as metallic delafossites $PdCoO_2$ and $PtCoO_2$ [10].

The salient feature in our work is that the AM after a coordinate transformation [11] is similar to Kerr metric [12] in Eddington-Finkelstein (EF) coordinates [13]. Recently, there have been several attempts to construct analog models of BHs other than the nonrotating ones [14–17]. The fluid, with the presence of a vortex in it, has been considered as a system to construct an analog of a rotating BH [14]. In [15], authors reasoned that in a shallow water system, with a varying background flow velocity, metric analogs of Kerr metric can be constructed. Later, the presence of superradiance was found in it [16] and also in the Bose-Einstein condensate [17]. In a recent work in this direction but exploiting the optical vortex is [18], the authors have used Laguerre-Gaussian-type beams, bearing phase singularities. These types of beams have transverse intensity profiles comprising all characteristics of a vortex. The fluctuations in the amplitude and the phase of the electric field have been shown to satisfy a

*surojitdalui@shu.edu.cn
†arpankmitra@aries.res.in
‡deeshani1997@gmail.com
§subirghosh20@gmail.com

massless scalar field equation on a curved background, similar to the Kerr metric. However, this present paper is possibly the first instance of an analog Kerr metric in the fluid subjected to an external magnetic field and Berry curvature. However, it is not unexpected since a spinlike feature appears in Berry curvature-modified particle dynamics [19]. The physics behind this AM is revealed through explicit construction of Kerr-like parameters, such as effective mass $m_{\rm eff}$ and angular momentum per unit mass $a_{\rm eff}$, out of fluid composites via dimensional analysis. More interestingly, using a specific form of nonuniform background fluid velocity we explicitly provide spatial positions of the ergoregion and horizon, characteristic of the Kerr metric.[1] Recently, multiple articles have shown studies on the trajectories of Weyl fermions in curved spacetimes [20–22]. One of them presented the trajectory of the massless Weyl particles around an analog Schwarzschild black hole [22]. Here we depict the phase space trajectories of a probe particle around the (Berry curvature-induced) analog Kerr metric that we have found and point out that the location of the analog horizon in this analog Kerr metric is the same as that of one in the Kerr metric in general relativity.

II. AM WITH BERRY CURVATURE EFFECTS

We consider a fluid with pressure $P(\rho)$. e is electronic charge, $\mathbf{B}$ external magnetic field and $\mathbf{\Omega}(\mathbf{k})$ is Berry curvature in momentum $(\bar{k})$ space. For small $\mathbf{\Omega}(\mathbf{k})$ the extended fluid model [with full expressions [6] in the Supplemental Material Eqs. (1)–(3)] is $[\mathcal{A}(\mathbf{x},\mathbf{k}) = 1 + e\mathbf{B}(\mathbf{x})\cdot\mathbf{\Omega}(\mathbf{k})]$

$$\dot{\rho} = -\nabla\left(\frac{\rho\mathbf{v}}{\mathcal{A}}\right), \tag{1}$$

$$\dot{\mathbf{v}} + \frac{(\mathbf{v}\cdot\boldsymbol{\nabla})\mathbf{v}}{\mathcal{A}} = -\frac{\boldsymbol{\nabla}P}{\rho\mathcal{A}}. \tag{2}$$

Irrotational $\mathbf{v} = -\nabla\psi$ is written by a velocity potential ψ. The velocity c_s of sonic disturbance in the medium and the system enthalpy h are $c_s = \sqrt{\frac{dP}{d\rho}}, \nabla h = \nabla P/\rho$ and (2) becomes

$$-\nabla\dot{\psi} + \nabla\left[\frac{(\nabla\psi)^2}{2\mathcal{A}}\right] = -\nabla\frac{h}{\mathcal{A}} \to \dot{\psi} - \frac{(\nabla\psi)^2}{2\mathcal{A}} = \frac{h}{\mathcal{A}}. \tag{3}$$

With the fluid variables as $background + fluctuation$ [2],

$$\rho = \rho_0 + \epsilon\rho_1, \quad P = P_0 + \epsilon c_s^2\rho_1,$$
$$v_i = v_{0i} + \epsilon v_{1i} = \partial_i\psi_0 + \epsilon\partial_i\psi_1, \quad \nabla h_1 = c_s^2\nabla\rho_1/\rho_0. \tag{4}$$

[1]We thank the anonymous referee for the suggestion.

the first-order perturbation terms are

$$\rho_1 = \left(\frac{\rho_0\dot{\psi}_1}{c_s^2}\right) + \left(\frac{\rho_0\overrightarrow{v_0}\cdot\nabla\psi_1}{c_s^2\mathcal{A}}\right), \tag{5}$$

$$\dot{\rho}_1 = -\frac{1}{\mathcal{A}}\nabla.(\rho_1\overrightarrow{v_0} - \rho_0\nabla\psi_1). \tag{6}$$

Taking the time derivative of (5) and comparing it with (6), (keeping external parameters and c_s fixed), we arrive at the wave equation of massless relativistic scalar in a curved spacetime,

$$\partial_\mu(f^{\mu\nu}\partial_\nu\psi_1) = 0,$$
$$f^{\mu\nu} = \frac{\rho_0}{c_s^2}\begin{pmatrix} \mathcal{A} & v_x & v_y & v_z \\ v_x & \frac{v_x^2-c_s^2}{\mathcal{A}} & \frac{v_xv_y}{\mathcal{A}} & \frac{v_xv_z}{\mathcal{A}} \\ v_y & \frac{v_xv_y}{\mathcal{A}} & \frac{v_y^2-c_s^2}{\mathcal{A}} & \frac{v_yv_z}{\mathcal{A}} \\ v_z & \frac{v_xv_z}{\mathcal{A}} & \frac{v_yv_z}{\mathcal{A}} & \frac{v_z^2-c_s^2}{\mathcal{A}} \end{pmatrix}. \tag{7}$$

Note that $f^{\mu\nu}$ depends on the background velocity v_{0i} which we write as v_i. The effective background metric $g^{\mu\nu}$ is $f^{\mu\nu} = \sqrt{-g}g^{\mu\nu}$ with the determinant of $f^{\mu\nu}$ given by $|f^{\mu\nu}| = (\sqrt{-g})^4\frac{1}{g} = g = -\frac{\rho_0^4}{c_s^2\mathcal{A}^2}$. The AM is constructed out of background fluid velocity and inherits symmetries of the latter. The AM is stationary as flow is stationary (or steady in fluid dynamics terminology). Thus, cherished AM $g_{\mu\nu}$, one of our major results, in polar form is

$$g_{\mu\nu} = \frac{\rho_0}{\mathcal{A}c_s}\begin{pmatrix} \frac{c_s^2-(v_r^2+v_\theta^2+v_\phi^2)}{\mathcal{A}} & v_r & rv_\theta & r\sin\theta v_\phi \\ v_r & -\mathcal{A} & 0 & 0 \\ rv_\theta & 0 & -\mathcal{A}r^2 & 0 \\ r\sin\theta v_\phi & 0 & 0 & -\mathcal{A}r^2\sin^2\theta \end{pmatrix}.$$

It is important to remember that fluid particles see the flat Minkowski metric (for fluid velocity $\ll$ velocity of the electromagnetic field in vacuum) whereas acoustic fluctuations feel only the AM; some basic properties of the latter carry a legacy of the former. From the above AM it is clear [23] that the regions of supersonic flow are ergoregions where g_{tt} changes sign, $g_{tt} = 0 \to v_r = c_s$ corresponds to the event horizon (wave-blocking zone in fluid dynamics); the boundary that null geodesics (or phonons) cannot escape. In fact, here the ergosphere coincides with the event horizon. Other notions such as trapped surface, surface gravity, etc also exist for AM [23]. Spatial positions of the analog horizon in the fluid will appear indirectly from $c_s(r), v_r(r)$.

III. $m_{\rm eff}$, $a_{\rm eff}$ IN AM-KERR ANALOGY

For matching with Kerr, we convert the acoustic path-length dimension to $|ds^2| = (\text{length})^2 = [L]^2$. In GR, the metrics have dimensional parameters such as Newton's constant G and velocity of light c, among others. Similarly, AM can depend on c_s, background fluid density ρ_0 (both not constant in general), etc. Another fluid parameter is the dynamic (or absolute) viscosity μ of dimension of $|\mu| = [M][L]^{-1}[T]^{-1}$ (with kinematic viscosity being μ/ρ_0). A length scale l ($\sim$ spatial dimension of the fluid system) enters our acoustic model. $\mathbf{k}$-dependence in $\mathbf{\Omega}(\mathbf{k})$ refers to the quasimomentum of a single band (in the crystalline solid) of the Bloch electron, comprising the electron fluid in the hydrodynamic limit, where the AM is constructed. For the present work, $\mathbf{k}$ is just a label and is treated as a constant. For a uniform $\mathbf{B}(\mathbf{r}) = \mathbf{B}$, $\mathcal{A}$ is effectively a constant. The resulting acoustic path has $|ds^2_{\rm AM}| = (\text{length})^2$ dimension,

$$ds^2_{\rm AM} = \frac{c_s l\rho_0}{\mu\mathcal{A}}\left[\frac{(c_s^2-v^2)}{\mathcal{A}}dt^2 + 2v_r dtdr + 2rv_\theta dtd\theta + 2r\sin\theta v_\phi dtd\phi - \mathcal{A}\{dr^2 + r^2d\theta^2 + r^2\sin^2\theta d\phi^2\}\right], \tag{8}$$

where $v^2 = v_r^2 + v_\theta^2 + v_\phi^2$. Now we perform a coordinate transformation

$$dt \to dt + \frac{dr}{c_s} + \frac{d\theta}{\omega_s} + \frac{d\phi}{\Omega_s},$$
$$\omega_s = \text{angular frequency},$$
$$\Omega_s = \text{azimuthal frequency of sonic disturbance}, \tag{9}$$

on the acoustic path to obtain,

$$\begin{aligned} ds^2_{\rm AM} = \frac{c_s l\rho_0}{\mu\mathcal{A}}\Bigg[&\frac{(c_s^2-v^2)}{\mathcal{A}}dt^2 + \left\{\frac{(c_s^2-v^2)}{\mathcal{A}c_s^2} + \frac{2v_r}{c_s^2} - \mathcal{A}\right\}dr^2 + 2\left\{\frac{(c_s^2-v^2)}{\mathcal{A}c_s} + v_r\right\}dtdr + 2\left\{\frac{(c_s^2-v^2)}{\mathcal{A}\Omega_s} + r\sin\theta v_\phi\right\}dtd\phi \\ &+ 2\left\{\frac{(c_s^2-v^2)}{\mathcal{A}\omega_s} + rv_\theta\right\}dtd\theta + 2\left\{\frac{(c_s^2-v^2)}{\mathcal{A}c_s} + \frac{v_r}{\omega_s} + \frac{rv_\theta}{c_s}\right\}drd\theta + 2\left\{\frac{(c_s^2-v^2)}{\mathcal{A}\Omega_s\omega_s} + \frac{r\sin\theta v_\phi}{\omega_s} + \frac{rv_\theta}{\Omega_s}\right\}d\theta d\phi \\ &+ 2\left\{\frac{(c_s^2-v^2)}{\mathcal{A}c_s\Omega_s} + \frac{v_r}{\Omega_s} + \frac{r\sin\theta v_\phi}{c_s}\right\}drd\phi + \left\{\frac{(c_s^2-v^2)}{\mathcal{A}\Omega_s^2} - \mathcal{A}r^2\sin^2\theta + \frac{2r\sin\theta}{\Omega_s}v_\phi\right\}d\phi^2 \\ &+ \left\{\frac{(c_s^2-v^2)}{\mathcal{A}\omega_s^2} - \mathcal{A}r^2 + \frac{2r}{\omega_s}v_\theta\right\}d\theta^2\Bigg]. \end{aligned} \tag{10}$$

Our major observation is that in the equatorial plane (i.e., $\theta = \pi/2$ hypersurface) and with $v_\theta = 0$, the acoustic path,

$$\begin{aligned} ds^2_{\rm AM} = \frac{c_s l\rho_0}{\mu\mathcal{A}}\Bigg[&\frac{(c_s^2-v^2)}{\mathcal{A}}dt^2 + \left\{\frac{(c_s^2-v^2)}{\mathcal{A}c_s^2} + \frac{2v_r}{c_s^2} - \mathcal{A}\right\}dr^2 + 2\left\{\frac{(c_s^2-v^2)}{\mathcal{A}c_s} + v_r\right\}dtdr + 2\left\{\frac{(c_s^2-v^2)}{\mathcal{A}\Omega_s} + rv_\phi\right\}dtd\phi \\ &+ 2\left\{\frac{(c_s^2-v^2)}{\mathcal{A}c_s\Omega_s} + \frac{v_r}{\Omega_s} + \frac{rv_\phi}{c_s}\right\}drd\phi + \left\{\frac{(c_s^2-v^2)}{\mathcal{A}\Omega_s^2} - \mathcal{A}r^2 + \frac{2r}{\Omega_s}v_\phi\right\}d\phi^2\Bigg], \end{aligned} \tag{11}$$

is structurally equivalent to Kerr metric path length in Eddington-Finklestein coordinates [full expressions in Supplemental Material Eqs. (5)–(10)],

$$\begin{aligned} ds^2_{\rm Kerr} = &\left(1 - \frac{2Gm}{rc^2}\right)c^2dt^2 - \frac{4Gm}{rc}dtdr + \frac{4Gma}{rc^2}dtd\phi - \left(1 + \frac{2Gm}{rc^2}\right)dr^2 + 2\frac{a}{c}\left(1 + \frac{2Gm}{rc^2}\right)drd\phi \\ &- \left(r^2 + \frac{a^2}{c^2} - \frac{2Gma^2}{rc^4}\right)d\phi^2. \end{aligned} \tag{12}$$

We exploit the dimensional equality $ds^2_{\rm AM} = ds^2_{\rm Kerr} = (\text{length})^2$ to construct effective mass and spin parameters for AM, in analogy with mass (m) and angular momentum per unit mass $a = J/m$ of Kerr black hole [with details in Supplemental Material Eqs. (11)–(17)]:

(i) Comparison of the dimensions of g_{tt} gives

$$m_{\rm eff} \equiv \frac{l^3\rho_0 v^2}{\mathcal{A}^2 c_s^2} \tag{13}$$

and

(ii) Comparison of the dimensions of $g_{t\phi}$ gives

$$a_{\rm eff} \equiv \frac{l\rho_0 c_s^5}{\mu \mathcal{A}^2 \Omega_s v^2}. \tag{14}$$

This constitutes another set of important results since these effective parameters are, in principle, measurable.

In terms of $m_{\rm eff}$ and $a_{\rm eff}$ the same metric (11) turns out to be

$$\begin{aligned} ds^2_{\rm AM} = &\left(\frac{c_s l\rho_0}{\mu\mathcal{A}^2} - m_{\rm eff}\frac{c_s}{\mu l^2}\right)c_s^2 dt^2 + 2m_{\rm eff}\frac{c_s^2}{\mu l^2}\left(\frac{c_s^2}{v^2} - 1 + \frac{c_s v_r \mathcal{A}}{v^2}\right)dtdr + 2m_{\rm eff}a_{\rm eff}\left(\frac{\mathcal{A}^2}{l^3\rho_0}\right)\left(1 - v^2 + \frac{\Omega_s \mathcal{A}}{c_s^2} r v_\phi\right)dtd\phi \\ &+ \left[\frac{c_s l\rho_0}{\mu\mathcal{A}^2}\left(1 + 2\frac{v_r}{c_s^2}\mathcal{A} - \mathcal{A}^2\right) - m_{\rm eff}\frac{c_s}{\mu l^2}\right]dr^2 + 2a_{\rm eff}\frac{v_r^2}{c_s^3}\left[1 - m_{\rm eff}\frac{\mathcal{A}^2}{l^3\rho_0 c_s} + \frac{\mathcal{A}v_r}{c_s} + \frac{\mathcal{A}\Omega_s}{c_s^2} r v_\phi\right]drd\phi \\ &+ \left[\frac{\mu\mathcal{A}^2 v^4}{c_s^7 l\rho_0}a_{\rm eff}^2\left(1 - m_{\rm eff}\frac{\mathcal{A}^2}{l^3\rho_0}\right) - \frac{c_s l\rho_0}{\mu} r^2 + 2\frac{c_s l\rho_0}{\mu\mathcal{A}\Omega_s} r v_\phi\right]d\phi^2. \end{aligned} \tag{15}$$

Remarkably, our entirely algebraic methodology for implementing coordinate transformations (10) and prescription of identifying fluid mass and spin parameters have resulted in an AM (15), which can be compared term by term with the Kerr metric (see Supplemental Material [24]). Notice that $m_{\rm eff}, a_{\rm eff}$ in AM (15) occupy identical positions as m, a in Kerr metric (see Supplemental Material [24]). This provides a mathematical consistency of our framework and reveals the physics behind AM.

IV. PHASE SPACE PROBE TRAJECTORY

The AM at $\theta = \pi/2$ has a timelike Killing vector $\chi^a = (1, 0, 0, 0)$ with conserved energy of a particle given by $E = -\chi^a p_a = -p_t$, where $p_a = (p_t, p_r, p_\theta, p_\phi)$. Using the AM in the dispersion relation $g^{ab}p_a p_b = -M^2$ for a particle of mass M in AM (with $p_\theta = 0$), particle energy E is obtained in terms of the other momentum components, as the positive energy root. Hamilton's equations of motion are

$$\dot{r} = \frac{\partial E}{\partial p_r}, \quad \dot{p}_r = -\frac{\partial E}{\partial r}, \quad \dot{\phi} = \frac{\partial E}{\partial p_\phi}, \quad \dot{p_\phi} = -\frac{\partial E}{\partial \phi}. \tag{16}$$

Let us consider a particular background fluid profile known as "draining bathtub" flow (for details see [23])

$$\mathbf{v} = \frac{A\hat{r} + B\hat{\phi}}{r}. \tag{17}$$

with constant A, B. In this idealized model, background fluid flow is planar until it reaches a linear sink along perpendicular direction. The background fluid density ρ is taken to be constant throughout the flow. Furthermore, for the barotropic fluid considered here, (2) and specific enthalpy (h) indicate that the background pressure P and the speed of sonic disturbance c_s are also constant. The equation of continuity (1), in cylindrical coordinates with a sink along z-direction, reduces to

$$\frac{1}{r}\left(\frac{\partial}{\partial r}(rv_r) + \frac{\partial v_\phi}{\partial \phi} + \frac{\partial}{\partial z}(rv_z)\right) = 0, \tag{18}$$

and clearly the profile (17) (with $v_z = 0$ on the plane just away from the sink and planar distance r measured from z-axis) is a solution of (18) (for more details, see Sec. 2.4.3 of [23]).

In this model the acoustic ergosphere and event horizon form at

$$r_{\rm ergosphere} = \frac{\sqrt{A^2 + B^2}}{c_s}, \qquad r_{\rm horizon} = \frac{|A|}{c_s}. \tag{19}$$

However, one important thing needs be to mentioned here is that the distinction between ergosphere and the acoustic horizon is critical for this model [23]. Therefore, keeping that in mind, we proceed here to solve these coupled differential equations numerically [Eqs. (16)].

After the numerical solutions we have plotted the phase-space plot between the radial coordinate (r) and the corresponding radial momentum of the particle (p_r). Depending on the sign of A (+ and −) we plot two cases. The values of the other parameters are as follows: $\mathcal{A} = 5$, $c_s = 100, \Omega_s = 1.0, \Gamma = \frac{c_s l\rho_0}{\mu\mathcal{A}} = 100$. In the first figure, i.e., Fig. 1 the amplitudes of the velocity components (i.e., v_r and v_ϕ) are respectively $A = B = 100,000$. In Fig. 1, we can see, that the phase-space trajectory of the particle starts with some lower-momentum value for a larger value of r, but as r decreases, the corresponding radial momentum value (p_r) increases and at $r = 1000$ the momentum reaches its maximum value. This nature of the graph depicts that as the particle moves near to $r = 1000$ the particle experiences a "sudden change" in its trajectory.

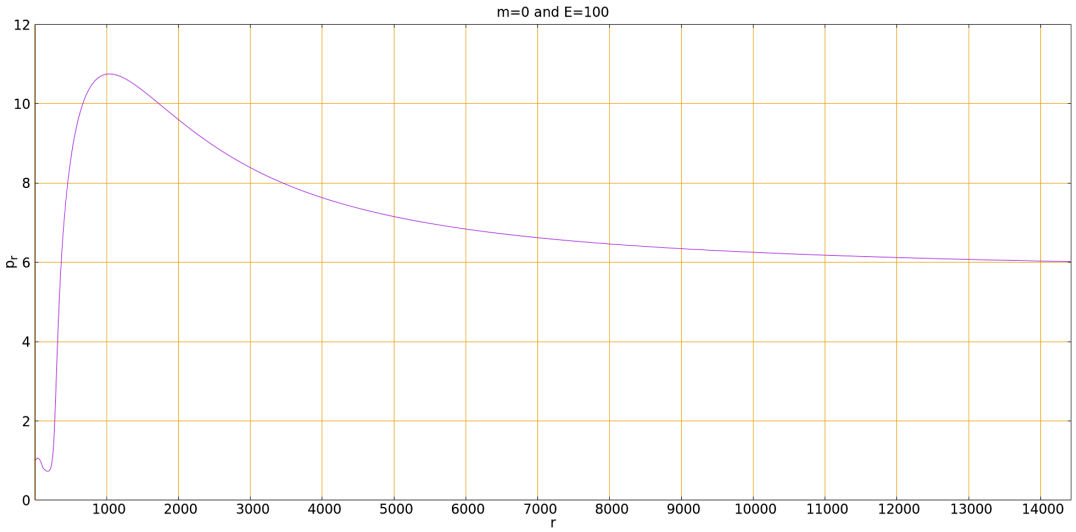

FIG. 1. Phase-space diagram for a massless particle (for $A = B = 1,000,000$). From the figure we can see as the particle moves near to $r = 1000$ its radial momentum p_r increases exponentially reaching its peak as r attains the value of 1000. This occurrence enables us to pinpoint the horizon's position, which precisely corresponds to the theoretical expectation at $|A|/c_s = 1000$.

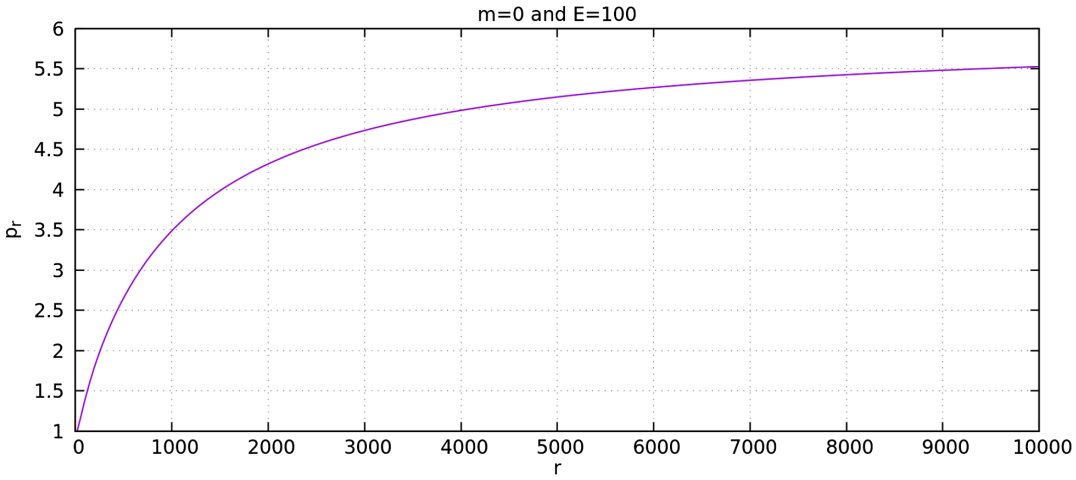

FIG. 2. Similarly, for $A = -100,000$ and $B = 500$ we plot again plot the phase-space trajectory of the massless particle remaining other parameter values the same. We see that until around $r \simeq 2000$ the radial momentum of the particle does not change much, but near to $r \simeq 1000$ the momentum of the particle suddenly falls down which suggests that the massless particle falls inside the horizon.

Moreover, according to the "draining bathtub" model the acoustic horizon should appear at $r = 1000$ [see Eq. (19)] which exactly happens in our case based on our specified parameter values. Consequently, from this occurrence, we can identify the position of the horizon, which exactly matches the theoretical value of the horizon, i.e., at $|A|/c_s = 1000$. In this context, it is worth mentioning that in some near-horizon contexts [13,25,26] it has been shown that in the near-horizon region, a particle experiences this kind of "sudden change" or "instability" in its phase-space trajectory.

Similarly, in Fig. 2 we have chosen $A = -100,000$ and $B = 500$ keeping the other parameters the same and we find that the radial momentum value of the massless particle does not change much until reaching $r \simeq 2000$. After $r \simeq 1000$ the momentum value falls abruptly which suggests that the particle is sucked inside the horizon which is situated at $r = 1000$. This characteristic is exactly similar to an ingoing massless particle in the near-horizon region of a SSS BH [see Eq. (26) and Page 8 of [26]] and a Kerr BH (see Page 6 of Ref. [13]).

In a nutshell, we can say that with the radial-dependent background flow of fluid, we can construct an analog metric which mimics the exact structure of Kerr BH, and by studying the particle dynamics in this background we can pinpoint the exact location of the horizon for particular values. Future works will involve a more rigorous analysis with the full anomalous fluid dynamics and an arbitrary fluid flow. Attempts of laboratory demonstrations of this new analog black hole model will be worthwhile.

[1] C. Barceló, S. Liberati, and M. Visser, Analogue gravity, Living Rev. Relativity **14**, 1 (2011).

[2] W. G. Unruh, Experimental black-hole evaporation?, Phys. Rev. Lett. **46**, 1351 (1981).

[3] L.-P. Euvé, F. Michel, R. Parentani, T. G. Philbin, and G. Rousseaux, Observation of noise correlated by the Hawking effect in a water tank, Phys. Rev. Lett. **117**, 121301 (2016); J. Steinhauer, Observation of quantum Hawking radiation and its entanglement in ananalogue black hole, Nat. Phys. **12**, 959 (2016); J. R. Muńoz de Nova, K. Golubkov, V. I. Kolobov, and J. Steinhauer, Observation of thermal Hawking radiation and its temperature in an analogue black hole, Nature (London) **569**, 688 (2019); J. Drori, Y. Rosenberg, D. Bermudez, Y. Silbergerg, and U. Leonhardt, Observation of stimulated Hawking radiation in an optical analogue, Phys. Rev. Lett. **122**, 010404 (2019); M. Clovecko, E. Gažo, M. Kupka, and P. Skyba, Magnonic analog of black- and white-hole horizons in superfluid 3He-B, Phys. Rev. Lett. **123**, 161302 (2019); D. Vocke, C. Maitland, A. Prain, K. E. Wilson, F. Biancalana, E. M. Wright, F. Marino, and D. Faccio, Rotating black hole geometries in a two-dimensional photon superfluid, Optica **5**, 1099 (2018); D. D. Solnyshkov, C. Leblanc, S. V. Koniakhin, O. Bleu, and G. Malpuech, Quantum analogue of a Kerr black hole and the Penrose effect in a Bose–Einstein condensate, Phys. Rev. B **99**, 214511 (2019); R. Aguero-Santacruz and D. Bermudez, Hawking radiation in optics and beyond, Phil. Trans. R. Soc. A **378**, 20190223 (2020); J. Petty and F. König, Optical analogue gravity physics: Resonant radiation, Phil. Trans. R. Soc. A **378**, 20190231 (2020); U. Leonhardt, The case for a Casimir cosmology, Phil. Trans. R. Soc. A **378**, 20190229 (2020); M. J. Jacquet, T. Boulier, F. Claude, A. Maître, E. Cancellieri, C. Adrados, A. Amo, S. Pigeon, Q. Glorieux, A. Bramati, and E. Giacobino, Polariton fluids for analogue gravity physics, Phil. Trans. R. Soc. A **378**, 20190225 (2020); M. P. Blencowe and H. Wang, Analogue gravity on a superconducting chip, Phil. Trans. R. Soc. A **378**, 20190224 (2020); Avijit Bera and Subir Ghosh, Stimulated Hawking emission from electromagnetic analogue black hole: Theory and observation, Phys. Rev. D **101**, 105012 (2020); M. A. Anacleto, F. A. Brito, and E. Passos, Acoustic black holes and universal aspects of area products, Phys. Lett. A **380**, 1105 (2016).

[4] M. J. Jacquet, S. Weinfurtner, and F. König, The next generation of analoguegravity experiments, Phil. Trans. R. Soc. A **378**, 20190239 (2020).

[5] D. Chatterjee, B. S. Mazumder, and S. Ghosh, Turbulence characteristics, Applied Ocean Research **75**, 15 (2018).

[6] A. K. Mitra and S. Ghosh, Divergence anomaly and Schwinger terms: Towards a consistent theory of anomalous classical fluids, Phys. Rev. D **106**, L041702 (2022).

[7] C. Duval, Z. Horváth, P. A. Horváthy, L. Martina, and P. C. Stichel, Berry phase correction to electron density in solids and "exotic" dynamics, Mod. Phys. Lett. B **20**, 373 (2006); P. Gosselin, A. Bérard, and H. Mohrbach, Semiclassical diagonalization of quantum Hamiltonian and equations of motion with Berry phase corrections, Eur. Phys. J. B **58**, 137 (2007); M. C. Chang and Q. Niu, Berry phase, hyperorbits, and the hofstadter spectrum, Phys. Rev. Lett. **75**, 1348 (1995).

[8] S K. Das, D. Roy, and S. Sengupta, An electron fluid model for the lattice dynamics of metals, Pramana **8**, 117 (1977); R. Slavchov and R. Tsekov, Quantum hydrodynamics of electron gases, J. Chem. Phys. **132**, 084505 (2010); Marco Polini and Andre K. Geim, Viscous electron fluids, Phys. Today **73**, No. 6, 28 (2020).

[9] A. Lucas and Kin Chung Fong, Hydrodynamics of electrons in graphene, J. Phys. Condens. Matter **30**, 053001 (2018).

[10] Andy Mackenzie, Nabhanila Nandi, Seunghyun Khim, Pallavi Kushwaha, Philip Moll, and Burkhard Schmidt, Electronic hydrodynamics, L. Barletti J. Math. Ind. **6**, 7 (2016); Justin C. W. Song and Mark S. Rudner, Hydrodynamic equations for an electron gas in graphene, Proc. Natl. Acad. Sci. U.S.A. **113**, 4658 (2016); A. Avdoshkin, V. P. Kirilin, A. V. Sadofyev, and V. I. Zakharov, On consistency of hydrodynamic approximation for chiral media, arXiv:1402.3587v3; C. L. Gardner, The quantum hydrodynamic model for semiconductor devices, SIAM J. Appl. Math. **54**, 409 (1994).

[11] J. Natário, Painlevé—Gullstrand coordinates for the Kerr solution, Gen. Relativ. Gravit. **41**, 2579 (2009).

[12] Roy P. Kerr, Gravitational field of a spinning mass as an example of algebraically special metrics, Phys. Rev. Lett. **11**, 237 (1963).

[13] S. Dalui and B. R. Majhi, Horizon thermalization of Kerr black hole through local instability, Phys. Lett. B **826**, 136899 (2022); S. Dalui, Classical and Quantum Aspects of Near-Horizon Physics, http://gyan.iitg.ernet.in/bitstream/handle/123456789/2319/TH-2995_176121013.pdf.

[14] M. Visser, Acoustic black holes: Horizons, ergospheres and Hawking radiation, Classical Quantum Gravity **15**, 1767 (1998).

[15] R. Schützhold and W. G. Unruh, Gravity wave analogues of black holes, Phys. Rev. D **66**, 044019 (2002).

[16] S. Weinfurtner, E. W. Tedford, M. C. J. Penrice, W. G. Unruh, and G. A. Lawrence, Measurement of stimulated hawking emission in an analogue system, Phys. Rev. Lett. **106**, 021302 (2011).

[17] T. R. Slayter and C. M. Savage, Superradiant scattering from a hydrodynamic vortex, Classical Quantum Gravity **22**, 3833 (2005).

[18] M. Ornigotti, S. Bar-Ad, A. Szameit, and V. Fleurov, Analog gravity by an optical vortex: Resonance enhancement of Hawking radiation, Phys. Rev. A **97**, 013823 (2018).

[19] S. Ghosh, Noncommutativity in Maxwell-Chern-Simons-Matter theory simulates pauli magnetic coupling, Mod. Phys. Lett. A **20**, 1227 (2005).

[20] A. Haller, S. Hegde, C. Xu, C. De Beule, T. L. Schmidt, and T. Meng, Black hole mirages: Electron lensing and Berry curvature effects in inhomogeneously tilted Weyl semimetals, SciPost Phys. **14**, 119 (2023).

[21] S. Guan, Z.-M. Yu, Y. Liu, G.-B. Liu, L. Dong, Y. Lu, Y. Yao, and S. A. Yang, Artificial gravity field, astrophysical analogues, and topological phase transitions in strained topological semimetals, npj Quantum Mater. **2**, 23 (2017).

[22] G. E. Volovik, Black hole and Hawking radiation by type-II Weyl fermions, JETP Lett. **104**, 645 (2016).

[23] M. Visser, Acoustic black holes: Horizons, ergospheres and Hawking radiation, Classical Quantum Gravity **15**, 1767 (1998); C. Barcelo, S. Liberati, and M. Visser, Analogue gravity, Living Rev. Relativity **8**, 12 (2005).
[24] See Supplemental Materials at http://link.aps.org/supplemental/10.1103/PhysRevD.109.064055 for more details.
[25] S. Dalui, B. R. Majhi, and P. Mishra, Horizon induces instability locally and creates quantum thermality, Phys. Rev. D **102**, 044006 (2020).
[26] S. Dalui and B. R. Majhi, Near horizon local instability and quantum thermality, Phys. Rev. D **102**, 124047 (2020).